Transient Radio Signatures from Neutron Star Encounters with QCD Axion Miniclusters

Edwards, T.D.P; Kavanagh, B.J.; Visinelli, L.; Weniger, C.

DOI
10.1103/PhysRevLett.127.131103

Publication date
2021

Document Version
Other version

Published in
Physical Review Letters

Transient Radio Signatures from Neutron Star Encounters with QCD Axion Miniclusters

Supplemental Material

Thomas D. P. Edwards, Bradley J. Kavanagh, Luca Visinelli, and Christoph Weniger

A. Neutron Star Population

Considerable effort has been put into modelling the population of neutron stars (NSs) in the Milky Way (MW) [1, 2] given the sample of those we can actually observe (see for example those reported by the Australia Telescope National Facility pulsar catalogue [3]). We assume that the spatial distribution of millisecond pulsars in the MW can be used to approximate the corresponding distribution of *old* NSs, as in Ref. [4].

The MW hosts around 10^9 NSs [5], of which 20% have been unbound due to natal kicks [5]. Of these NSs, 60% are formed in the bulge and 40% in the disk [5, 6]. We normalize the spatial distributions in the bulge and in the disk assuming the total numbers $N_{\rm bulge} = 4.8 \times 10^8$ and $N_{\rm disk} = 3.2 \times 10^8$, respectively. We model the NS spatial distributions in terms of the galactocentric cylindrical coordinates $r_{\rm cyl}$ and $z_{\rm cyl}$, which describe the radial distance from the axis of symmetry and the height from the Galactic plane respectively. Here, we assume that the spatial distribution of NSs in the bulge tracks the stellar population. We fix this in the companion paper [7] as a truncated Power-law distribution [8, 9]

$$n_{\rm bulge}(r_{\rm cyl}, z_{\rm cyl}) = N_{\rm bulge}\, \frac{11.1}{\rm kpc^3}\, \frac{e^{-\left(r'/r_{\rm cut}\right)^2}}{(1 + r'/r_0)^{\lambda}}\,, \tag{S1}$$

where we use the parameters from Ref. [10], namely the core density $\rho_0^{\rm bulge} \approx 99.3\, M_\odot/{\rm pc}^3$, $r' = \sqrt{r_{\rm cyl}^2 + (z_{\rm cyl}/q)^2}$ with $q = 0.5$, the bulge cutoff $r_0 = 0.075\,{\rm kpc}$, the exponent $\lambda = 1.8$, and $r_{\rm cut} = 2.1\,{\rm kpc}$. The numerical factor 11.1 accounts for the integration of the NS density over the bulge volume. Note, that this choice differs from other literature on the subject in which a Hernquist profile is assumed [4].

We use a Lorimer profile to model the distribution of millisecond pulsars in the Galactic disk [11]

$$n_{\rm disk}(r_{\rm cyl}, z_{\rm cyl}) = N_{\rm disk}\, \frac{C^{B+2}\, e^{-C}}{4\pi\, r_\odot^2 \sigma_z\, \Gamma(B+2)} \left(\frac{r_{\rm cyl}}{r_\odot}\right)^B e^{-C\frac{r_{\rm cyl} - r_\odot}{r_\odot}}\, e^{-\frac{|z_{\rm cyl}|}{\sigma_z}}\,, \tag{S2}$$

with parameters that are obtained from a fit to the population of almost one hundred millisecond pulsars — these are taken from Table III of Ref. [12], namely $B = 3.91$, $C = 7.54$, and $\sigma_z = 0.76\,{\rm kpc}$.

We have not incorporated any decay mechanisms for the NS's magnetic field, such as ohmic dissipation [13], ambipolar diffusion [14, 15], or Hall drift [16]. We assume that all NSs have a mass of $M_{\rm NS} = 1.4\, M_\odot$ and radius $R_{\rm NS} = 10\,{\rm km}$.

B. Neutron Star Magnetosphere

Here, we use the Goldreich-Julian model [17] of the NS magnetosphere, for which the magnetic field along the axis of rotation $\hat{\eta}$ is

$$B_{\hat{\eta}}(r, \theta_{\rm obs}) = B_0 \left(\frac{R_{\rm NS}}{r}\right)^3 \frac{3\cos^2\theta_{\rm obs} - 1}{2}\,, \tag{S3}$$

where the radial dependence shows the typical dipole behavior falling as $\propto r^{-3}$. For simplicity, we have assumed that the magnetic field is aligned with the axis of rotation, which are both inclined at an angle $\theta_{\rm obs} \in [-\pi/2, \pi/2]$ with respect to the observer. Each NS in the population is described by a magnetic field strength at the poles B_0 and a period P which are drawn from log-normal distributions, with mean and dispersion given by $\log_{10}(B/{\rm G}) = 12.65$ and $\sigma_B = 0.55$ for the magnetic field strength [1, 2], and $\log_{10}(P/{\rm ms}) = 2.7$ and $\sigma_P = 0.34$ for the period [11].

Given the angular velocity vector of the NS $\boldsymbol{\Omega}$ with absolute value $\Omega = 2\pi/P$, the charged plasma in the magnetosphere at distance r has a number density [17]

$$n_c = \frac{2\Omega B_{\hat{\eta}}(r, \theta_{\rm obs})}{e} + \text{relativistic corrections}\,. \tag{S4}$$

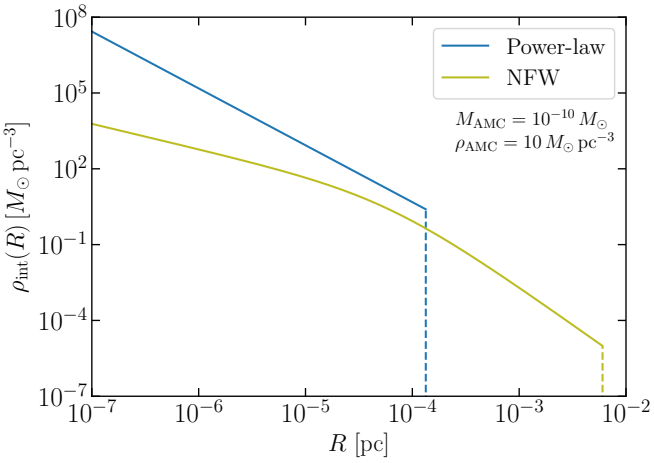

FIG. S1. Models for the internal density profile's of AMCs which we consider in this paper: Power-law, Eq. (S7), and NFW, Eq. (S9). Vertical dashed lines show the truncation radii $R_{\rm AMC}$. We fix the characteristic mass and density to $M_{\rm AMC} = 10^{-10}\,M_\odot$ and $\rho_{\rm AMC} = 10\,M_\odot\,{\rm pc}^{-3}$ respectively.

The plasma frequency can be expressed as $\omega_p = \sqrt{4\pi\alpha_{\rm EM} n_c/m_c}$ where $\alpha_{\rm EM}$ is the fine structure constant and m_c is the charge carrier mass. For electrons, we obtain

$$\omega_p = 150\,{\rm GHz}\sqrt{\left(\frac{B_{\tilde{\eta}}(r,\theta_{\rm obs})}{10^{14}\,{\rm G}}\right)\left(\frac{1\,{\rm s}}{P}\right)}\,. \tag{S5}$$

The conversion radius R_c is defined as the region for which the plasma frequency equals the axion mass. Using Eq. (S5), which is valid in the electron-dominated region, the conversion radius is given by [18]

$$R_c(\theta_{\rm obs}) = 224\,{\rm km}\left(\frac{R_{\rm NS}}{10\,{\rm km}}\right)\left[\left|3\cos^2\theta_{\rm obs} - 1\right|\frac{B_0}{10^{14}\,{\rm G}}\frac{1\,{\rm s}}{P}\left(\frac{1\,{\rm GHz}}{m_a}\right)^2\right]^{1/3}\,, \tag{S6}$$

where the resonant conversion only takes place if $R_c(\theta_{\rm obs}) > R_{\rm NS}$.

C. Axion Minicluster Density Profiles

As described in main text, we use two different parameterizations for the internal density profiles of the AMCs. Since we do not know the internal density profiles precisely, these two choices are made to reflect the range of potentially observable radio signatures. An example of both density profiles and their corresponding truncation radii can be seen in Fig. S1.

An AMC with a Power-law (PL) profile is described by [19, 20]

$$\rho_{\rm int}^{\rm PL}(R) = \rho_s\left(\frac{r_s}{R}\right)^{9/4}\Theta\left(R_{\rm AMC}^{\rm PL} - R\right)\,, \tag{S7}$$

where $\Theta(x)$ is the Heaviside step function. We truncate the PL profile at a radius

$$R_{\rm AMC}^{\rm PL} = \left(\frac{3M_{\rm AMC}}{4\pi\rho(\delta)}\right)^{1/3}\,, \tag{S8}$$

where we fix $\rho_s r_s^{9/4} = \rho(\delta)(R_{\rm AMC}^{\rm PL})^{9/4}/4$ [20], to give mean density $\rho(\delta)$ and the correct total mass for the AMC.

On the other hand, AMCs with NFW density profiles are described by

$$\rho_{\rm int}^{\rm NFW}(r) = \frac{\rho(\delta)}{(r/r_s)(1+r/r_s)^2}\,, \qquad r_s = \left(\frac{M_{\rm AMC}}{4\pi\rho(\delta)f_{\rm NFW}(c)}\right)^{1/3}\,, \tag{S9}$$

where the function $f_{\rm NFW}(c) = \ln(1+c) - c/(1+c)$ is defined in terms of a concentration parameter $c \approx 100$ [21, 22]. The truncation radius is now given by $R_{\rm AMC}^{\rm NFW} = c\,r_s$.

D. Flux Distributions

Here, we give more details concerning the expected distributions of radio fluxes from AMC-NS encounters. In the left panel of Fig. S2, we plot the cumulative probability distribution of the mean flux density $\langle \mathcal{S} \rangle$ (that is, the fraction of events above a given value of $\langle \mathcal{S} \rangle$). We show results for AMCs with Power-law (solid blue) and NFW (solid olive) internal density profiles. The typical flux density from an encounter between an NS and a Power-law minicluster is larger because these AMCs are substantially more dense than those with NFW profiles. We show also the results for AMCs which have not undergone perturbations due to stellar encounters (dashed lines). For Power-law miniclusters, these results are very similar to the perturbed case; their higher density also makes them more resistant to disruption. Instead, for NFW miniclusters, the typical flux which we would expect when neglecting perturbations is much smaller than when perturbations are included.

We can see this expressed also in terms of the encounter rate above a given threshold in flux $\langle \mathcal{S} \rangle$, as shown in the right panel of Fig. S2. In the NFW case, going from the perturbed to unperturbed distributions, the encounter rate drops by a factor of around 40. However, the rate of very bright encounters actually *increases* once perturbations are taken into account. As we show in detail in Ref. [7], the survival probability for NFW miniclusters is typically larger than 50% throughout the MW. However, surviving AMCs are stripped of a significant fraction of their mass, typically leaving behind a much more dense remnant AMC. Thus, what would be common encounters with large, diffuse AMCs in the unperturbed case become rarer but brighter encounters with small, dense AMCs once perturbations are accounted for.

Of particular interest is that for the very brightest events (above around 1 Jy) the NS encounter rates for Power-law and NFW miniclusters start to converge, typically to within an order of magnitude. Despite the substantial differences in their sizes and densities, we find that the rate of bright encounters between NSs and AMCs in the MW is somewhat insensitive to the initial density profiles of the AMCs.

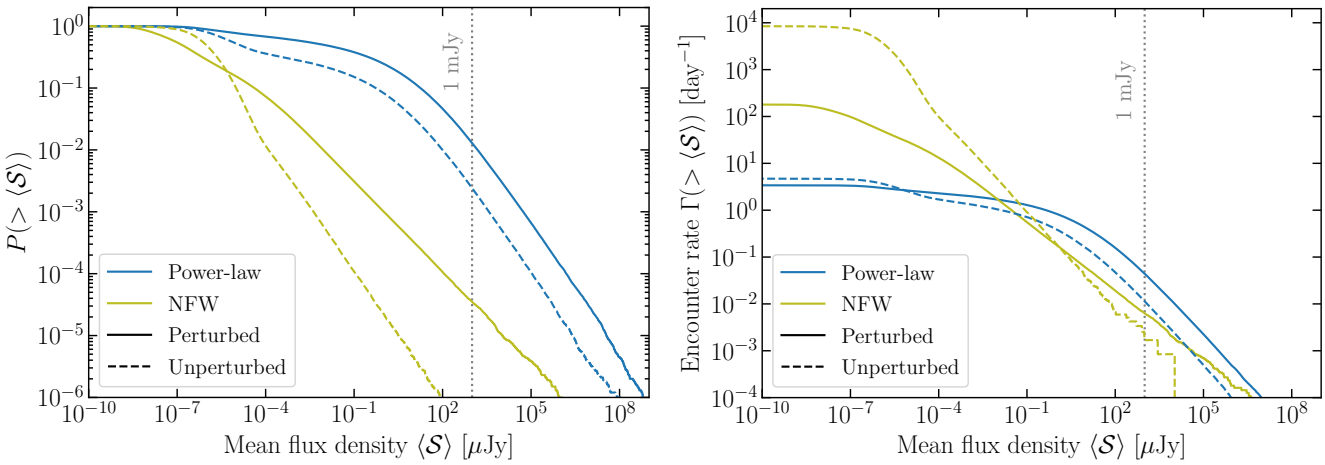

FIG. S2. *Left:* The cumulative probability of AMC-NS encounters as a function of the mean flux $\langle \mathcal{S} \rangle$ of the resulting radio signal. *Right:* Cumulative rate of encounters above a given mean flux $\langle \mathcal{S} \rangle$.

E. The Role of Axion Stars

An axion star (AS) [23] is a condensate made of cold axions, described by a solitonic solution of the relativistic Klein-Gordon equation [24, 25]. The axions inside the star are usually non-relativistic, so that a description in terms of the Schrödinger-Poisson (SP) equation is often a suitable approximation. Since axions are pseudo-scalar particles, ASs differ from the analogous solutions for 'boson stars' obtained in scalar boson theories [26]. While for scalar bosons a static solitonic solution to the SP exists, for pseudo-scalar axions the solution has to be oscillating periodically in time. An AS is then made up of a self-gravitating, oscillating axion field.

ASs may form in the dense central region of an axion minicluster, where the density is high enough that two-to-two processes enable the cooling of its inner core and lead to the formation of the condensate [27, 28]. This process has been observed in recent numerical simulations [29–31]. The existence of ASs could be indirectly probed through their

interaction with stellar objects, which leads to a vast array of potentially detectable signals in the form of gravitational waves, neutrinos, and electromagnetic radiation [32, 33].

Equilibrium in the so-called 'dilute' branch is granted by quantum pressure — due to the wave-like nature of the axions — which supports the AS from collapsing under its own self-gravity. Other branches in which gravity is replaced by self-interactions have been shown to be unstable or even non-existing [34]. For this reason, we limit our discussion to the dilute branch, in which the radius of the AS scales inversely with the AS mass, $R_{\rm AS} \propto M_{\rm AS}^{-1}$, a relation which can be inferred from energy conservation arguments [34]. The proportionality constant must be determined by numerically solving the SP equation. References [30, 35] find

$$R_{\rm AS} = 3.85 \times 10^{-8}\,{\rm m} \left(\frac{20\,\mu{\rm eV}}{m_a}\right)^2 \left(\frac{M_\odot}{M_{\rm AS}}\right) . \tag{S10}$$

Simulations of DM with wave-like properties of dwarf galaxy scales suggest a relation between the mass of the solitonic core and the mass of its host halo [35]. This relation has recently been confirmed for heavier axion-like particles, as we consider here, suggesting that ASs formed at the center of AMCs have a mass:

$$M_{\rm AS} = 1.56 \times 10^{-13}\,M_\odot \left(\frac{20\,\mu{\rm eV}}{m_a}\right) \left(\frac{M_{\rm AMC}}{1\,M_\odot}\right)^{1/3} . \tag{S11}$$

Combining Eqs. (S10) and (S11), we can write:

$$R_{\rm AS} = R_\star \left(\frac{M_{\rm AMC}}{M_\star}\right)^{-1/3} , \tag{S12}$$

where for $m_a = 20\,\mu$eV we fix the constants $R_\star = 1.7 \times 10^{-6}\,$pc and $M_\star = 10^{-16}\,M_\odot$. While current numerical simulations cannot resolve the formation of ASs in the smallest AMCs we consider, we will assume that Eq. (S12) holds generally.

The presence of ASs in the centers of AMCs may affect their behaviour under stellar perturbations. We neglect this effect, which should be small for the heaviest AMCs. More dramatically, at sufficiently low AMC mass, the radius of the AS formed at the center may exceed the radius of the AMC itself. We remain agnostic about the formation and behaviour of these light AMCs and instead apply a cut (referred to as the 'AS cut' in Ref. [7]) which discards all AMCs for which the AS radius exceeds the AMC radius. More precisely, the AS cut therefore removes all AMCs for which:

$$R_f > R_{\rm AS}(M_i) = R_\star \left(\frac{M_i}{M_\star}\right)^{-1/3} , \tag{S13}$$

where M_i is the AMC mass before stellar perturbations are accounted for and R_f is the final AMC radius after perturbations. In the main text, we present results in which we begin with $f_{\rm AMC} = 1$ over the full range of AMC masses $[M_{\rm min}, M_{\rm max}]$, which then undergo stellar perturbations, followed by the AS cut. As a guide, the fraction of AMCs passing the AS cut *before* perturbations is $f_{\rm cut}^{\rm PL} = 2.7 \times 10^{-4}$ for PL density profiles and $f_{\rm cut}^{\rm NFW} = 1.5 \times 10^{-2}$ for NFW profiles.

[1] C.-A. Faucher-Giguere and V. M. Kaspi, Astrophys. J. **643**, 332 (2006), arXiv:astro-ph/0512585.
[2] S. Bates, D. Lorimer, A. Rane, and J. Swiggum, Mon. Not. Roy. Astron. Soc. **439**, 2893 (2014), arXiv:1311.3427 [astro-ph.IM].
[3] R. N. Manchester, G. B. Hobbs, A. Teoh, and M. Hobbs, Astron. J. **129**, 1993 (2005), arXiv:astro-ph/0412641.
[4] B. R. Safdi, Z. Sun, and A. Y. Chen, Phys. Rev. D **99**, 123021 (2019), arXiv:1811.01020 [astro-ph.CO].
[5] N. Sartore, E. Ripamonti, A. Treves, and R. Turolla, Astron. Astrophys. **510**, A23 (2010), arXiv:0908.3182 [astro-ph.GA].
[6] E. O. Ofek, Publ. Astron. Soc. Pac. **121**, 814 (2009), arXiv:0910.3684 [astro-ph.GA].
[7] B. J. Kavanagh, T. D. P. Edwards, L. Visinelli, and C. Weniger, (2020), arXiv:2011.05377 [astro-ph.GA].
[8] J. Binney, O. Gerhard, and D. Spergel, Mon. Not. Roy. Astron. Soc. **288**, 365 (1997), arXiv:astro-ph/9609066.
[9] N. Bissantz and O. Gerhard, Mon. Not. Roy. Astron. Soc. **330**, 591 (2002), arXiv:astro-ph/0110368.
[10] P. J. McMillan, Mon. Not. Roy. Astron. Soc. **414**, 2446 (2011), arXiv:1102.4340 [astro-ph.GA].
[11] D. R. Lorimer *et al.*, Mon. Not. Roy. Astron. Soc. **372**, 777 (2006), arXiv:astro-ph/0607640.
[12] R. T. Bartels, T. D. P. Edwards, and C. Weniger, Mon. Not. Roy. Astron. Soc. **481**, 3966 (2018), arXiv:1805.11097 [astro-ph.HE].

[13] P. Haensel, V. A. Urpin, and D. G. Iakovlev, Astron. Astrophys. **229**, 133 (1990).
[14] P. Goldreich and A. Reisenegger, Astrophys. J. **395**, 250 (1992).
[15] D. A. Shalybkov and V. A. Urpin, Mon. Not. Roy. Astron. Soc. **273**, 643 (1995).
[16] J. A. Pons and U. Geppert, Astron. Astrophys. **470**, 303 (2007), arXiv:astro-ph/0703267.
[17] P. Goldreich and W. H. Julian, Astrophys. J. **157**, 869 (1969).
[18] A. Hook, Y. Kahn, B. R. Safdi, and Z. Sun, Phys. Rev. Lett. **121**, 241102 (2018), arXiv:1804.03145 [hep-ph].
[19] C. A. J. O'Hare and A. M. Green, Phys. Rev. D **95**, 063017 (2017), arXiv:1701.03118 [astro-ph.CO].
[20] M. Fairbairn, D. J. E. Marsh, J. Quevillon, and S. Rozier, Phys. Rev. D **97**, 083502 (2018), arXiv:1707.03310 [astro-ph.CO].
[21] B. Eggemeier, J. Redondo, K. Dolag, J. C. Niemeyer, and A. Vaquero, Phys. Rev. Lett. **125**, 041301 (2020), arXiv:1911.09417 [astro-ph.CO].
[22] D. Ellis, D. J. E. Marsh, and C. Behrens, Phys. Rev. D **103**, 083525 (2021), arXiv:2006.08637 [astro-ph.CO].
[23] I. I. Tkachev, Phys. Lett. B **261**, 289 (1991).
[24] D. J. Kaup, Phys. Rev. **172**, 1331 (1968).
[25] R. Ruffini and S. Bonazzola, Phys. Rev. **187**, 1767 (1969).
[26] M. Colpi, S. L. Shapiro, and I. Wasserman, Phys. Rev. Lett. **57**, 2485 (1986).
[27] E. W. Kolb and I. I. Tkachev, Phys. Rev. Lett. **71**, 3051 (1993), arXiv:hep-ph/9303313.
[28] E. Seidel and W.-M. Suen, Phys. Rev. Lett. **72**, 2516 (1994), arXiv:gr-qc/9309015.
[29] D. G. Levkov, A. G. Panin, and I. I. Tkachev, Phys. Rev. Lett. **121**, 151301 (2018), arXiv:1804.05857 [astro-ph.CO].
[30] B. Eggemeier and J. C. Niemeyer, Phys. Rev. D **100**, 063528 (2019), arXiv:1906.01348 [astro-ph.CO].
[31] J. Chen, X. Du, E. W. Lentz, D. J. E. Marsh, and J. C. Niemeyer, (2020), arXiv:2011.01333 [astro-ph.CO].
[32] S. Raby, Phys. Rev. D **94**, 103004 (2016), arXiv:1609.01694 [hep-ph].
[33] T. Dietrich, F. Day, K. Clough, M. Coughlin, and J. Niemeyer, Mon. Not. Roy. Astron. Soc. **483**, 908 (2019), arXiv:1808.04746 [astro-ph.HE].
[34] L. Visinelli, S. Baum, J. Redondo, K. Freese, and F. Wilczek, Phys. Lett. B **777**, 64 (2018), arXiv:1710.08910 [astro-ph.CO].
[35] H.-Y. Schive, M.-H. Liao, T.-P. Woo, S.-K. Wong, T. Chiueh, T. Broadhurst, and W. Y. P. Hwang, Phys. Rev. Lett. **113**, 261302 (2014), arXiv:1407.7762 [astro-ph.GA].